CONF-961202--38 SAN096-1718C

MICROSTRUCTURE AND INTERFACIAL PROPERTIES OF LATERALLY OXIDIZED $Al_xGa_{1-x}As$

R.D. TWESTEN, D. M. FOLLSTAEDT, AND K. D. CHOQUETTE
Sandia National Laboratories, Albuquerque, NM. 87185-1056 rdtwest@sandia.gov

ABSTRACT

The oxidation of high Al content $Al_xGa_{1-x}As$ has received much attention due to its use in oxide-aperture, vertical-cavity surface emitting lasers (VCSELs) and for passivating AlAs against environmental degradation. We have recently identified the spinel, gamma phase of Al_2O_3 in layers laterally oxidized in steam at 450°C for x=0.98 & 0.92 and have seen evidence for an amorphous precursor to the gamma phase. At the interface with the unoxidized $Al_xGa_{1-x}As$, an ~17nm amorphous phase remains which could account for the excellent electrical properties of oxide-confined VCSELs and help reduce stress concentrations at the oxide terminus.

INTRODUCTION

It has long been known that AlAs is subject to environmental degradation due to its high reactivity. It was discovered that intentional oxidation of AlAs can passivate the surface against further oxidation[1] and that varying the Ga content of the film will drastically reduce the oxidation rate for this process[2]. This selective and passivating nature of oxidized AlGaAs has been incorporated into vertical-cavity surface emitting lasers (VCSELs) to form current-confining and optical-mode defining apertures, which have allowed the development of high-performance devices[3,4,5].

In this paper, we discuss the microstructure of the oxide phase formed from the wet oxidation of 2%- and 8%-Ga AlAs in actual working VCSEL device structures (Figure 1). It is found that the oxide phase formed is fine grained (~4nm) γ-Al_2O_3 surrounded by an amorphous matrix. This is consistent with early work of Sugg et al.[6] and the crystalline phase identified in wet oxidation of pure AlAs[7]. It is also found that the lateral oxidation front terminates with an ~17nm amorphous zone. Lattice images show that the oxide terminus has a smooth transition from crystalline to amorphous, and lower magnification, strain-contrast images reveal no defects associated with the oxidation front. This lack of defects occurs in spite of the fact that measured contraction of the oxidized layers is 6.3%, straining the unoxidized layers[8].

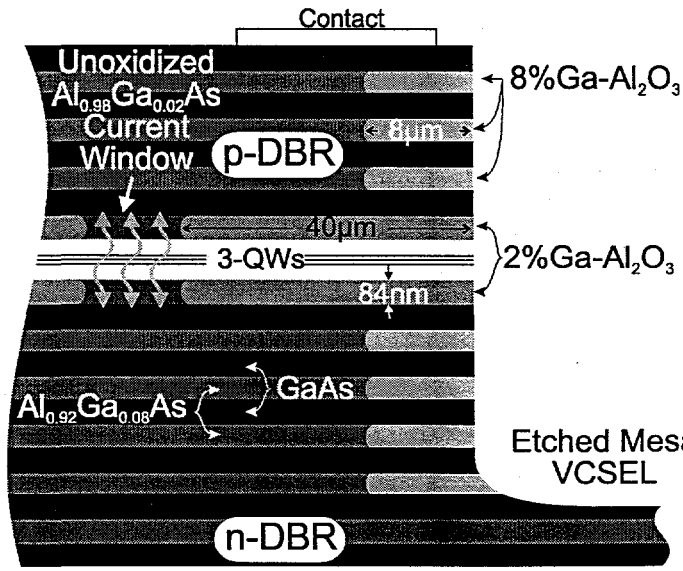

Figure 1: Schematic diagram of an oxide-confined, 980nm VCSEL device. Not to scale.

To Appear: MRS Fall 1996 Symposium M Proceedings

EXPERIMENTAL

Layers containing 2%- and 8%-Ga AlAs were laterally oxidized in a steam furnace at 450°C by bubbling N_2 through 80°C H_2O. The layers were part of working 980nm VCSEL devices. TEM cross-sectional samples were made by dicing the devices out of the wafer and epoxying them in a Si support stack. The stack was mechanically polished and then Ar-ion thinned so that the unoxidized current aperture of the device was thinned to electron transparency (see Figure 1). The final sample contained the oxide terminus of the 2%-Ga AlAs layers that define the current aperture in addition to the 8%-Ga AlAs layers that formed the remainder of the distributed Bragg reflector mirrors. The 8%-Ga layers only oxidize 8μm inward as compared to the 40μm oxidation of the 2%-Ga layers, due to the strong dependence of oxidation rate on Ga content[2]. TEM images were obtained using 200keV electrons and recorded either directly on to film or using a cooled, slow-scan video camera.

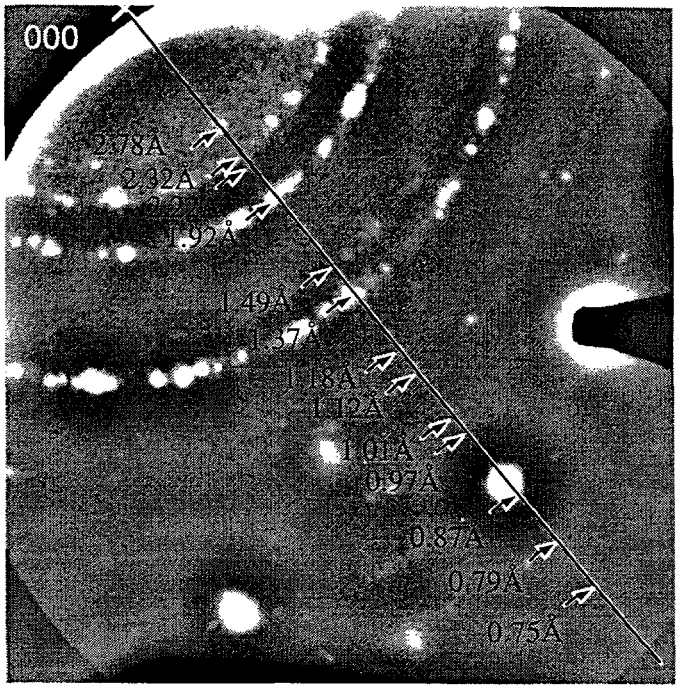

Figure 2: A portion of a selected area diffraction pattern of oxidized 2%Ga-AlAs. The image has been filtered to show detail. The sharp spots are from the unoxidized GaAs layers, while the rings are from the oxidized layer. The d-spacing for each ring is indicated.

RESULTS

Figure 2 shows a portion of an electron diffraction pattern which has been high-pass filtered to show the detail of the pattern. Clear polycrystalline rings can be seen in the pattern as well as an array of spots from the surrounding GaAs layers, which act as an internal calibration for the pattern. By measuring the ring spacing, the polycrystalline phase is identified as γ-Al_2O_3[9]. This is the cubic phase of Al_2O_3 and is based on the spinel ($MgAl_2O_4$) prototype with 32 O-atoms forming an FCC sublattice, 8 Al-atoms on the tetrahedral sites, and the remaining $13^1/_3$ Al-atoms on the octahedral sites leaving $6^2/_3$ octahedral vacancies[10]. The degree of ordering of

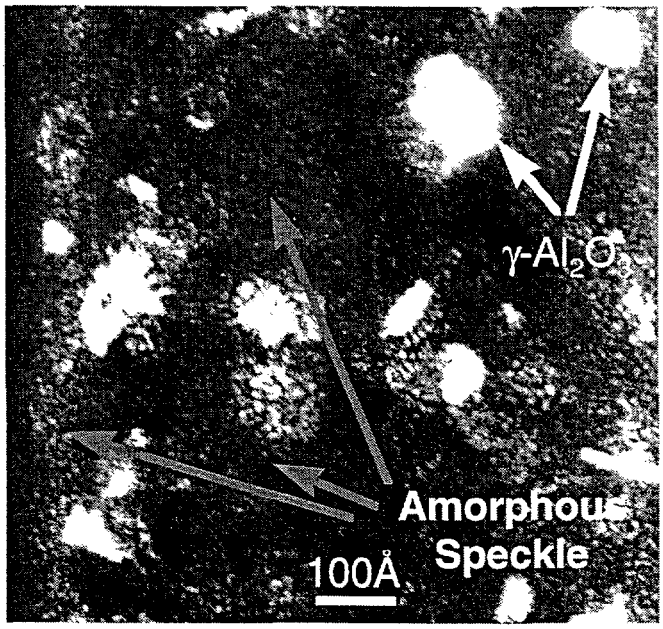

Figure 3: Dark-field g=(311) γ-Al_2O_3 image of oxidized 8%-Ga AlAs. The bright grains are γ-Al_2O_3 while the fine speckle between the grains is an amorphous phase.

the octahedral Al-atoms distinguishes the various forms of the cubic, transitional aluminas that we group together as the gamma phase. The gamma phase is formed by dehydration of $Al(OH)_3$ and AlO(OH). Upon high temperature processing, the gamma phase transforms into the hexagonal, alpha phase (sapphire).

At low concentrations, Ga_2O_3 forms solid solutions with Al_2O_3[11] and Ga_2O_3 has corresponding cubic and hexagonal phases. It is expected, therefore, that the Ga in the layers simply forms a solid solution of Ga_2O_3/Al_2O_3. This is supported by energy-dispersive x-ray spectroscopy (EDXS) that shows the Ga retained in the layer (see below) and the lack of any additional Ga-related phases in the diffraction pattern or images.

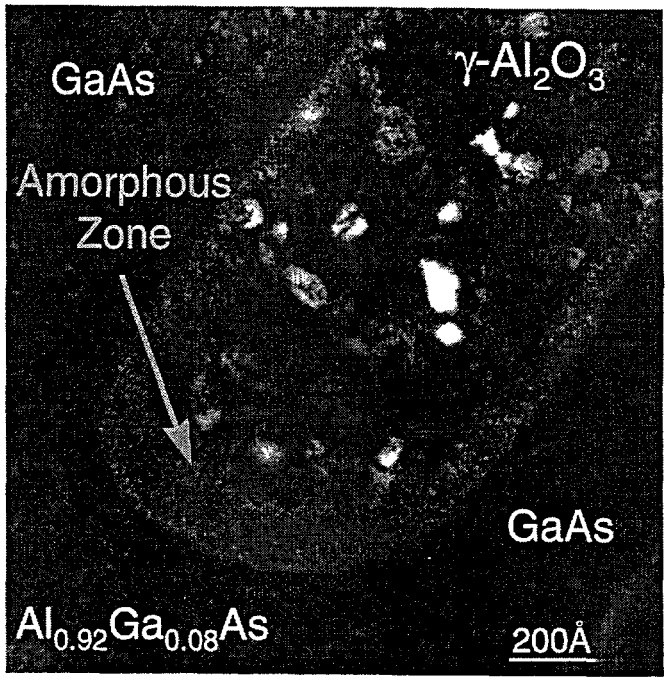

Figure 4: Dark-field image of the oxide terminus. Between the polycrystalline γ-Al_2O_3 and the unoxidized $Al_xGa_{1-x}As$, there is an ~17nm thick amorphous zone.

While the diffraction patterns show that the gamma phase is the only oxide present with long-range order, dark-field images suggest an amorphous matrix surrounding the crystalline phase. Figure 3 shows a dark-field image obtained using a portion of the (311) ring of the γ-Al_2O_3. The image shows the fine grain nature of the oxide with an average diameter of ~4nm. The orientation of the grains appears random, indicating precipitation from a random precursor rather directly from the AlGaAs lattice. In addition to the crystalline γ-Al_2O_3 grains, a fine speckle can be seen between the grains, which is typical of dark-field images of amorphous material. This amorphous phase could be an uncrystallized hydroxide, $Al(OH)_3$, or the amorphous ρ-alumina phase which forms in the vacuum dehydration of $Al(OH)_3$. It is likely that this amorphous phase forms as a precursor to the γ-Al_2O_3.

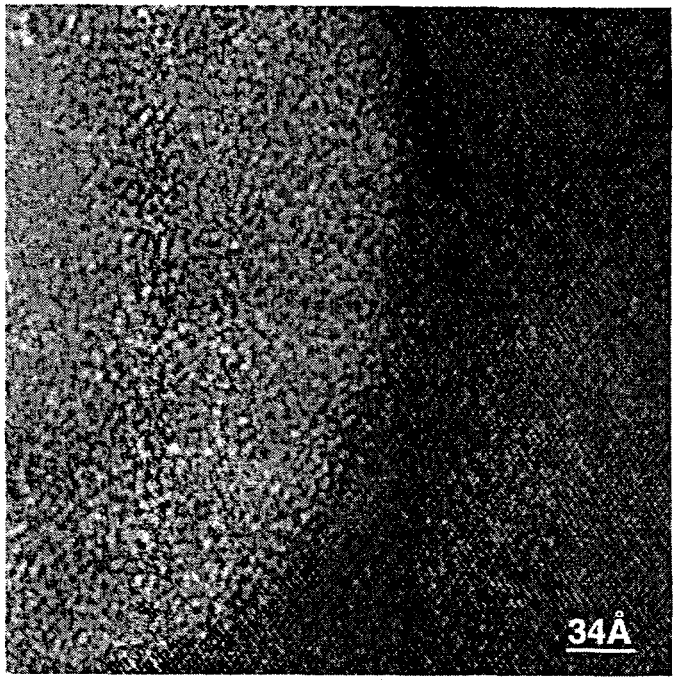

Figure 5: [110] Lattice image of the of the oxide terminus. The smooth transition from single crystal $Al_xGa_{1-x}As$ to amorphous oxide is seen. The transition from amorphous to polycrystalline oxide is seen on the left.

The suggestion that an amorphous oxide phase acts as a precursor to the gamma phase is also supported by the

existence of an amorphous interface region at the oxide terminus. Figure 4 shows a dark-field image of the oxide terminus of an 8%-Ga AlAs layer. The polycrystalline γ-Al_2O_3 can be seen in addition to the amorphous matrix. Also, at the interface with the unoxidized crystal, a 17nm-thick amorphous band can be seen. Bright-fields images also show granular amorphous contrast in this zone (see Figure 5). The tapering of this amorphous layer near the GaAs interfaces is a result of the intentional grading of the group III content at the $Al_xGa_{1-x}As$ /GaAs interfaces in the DBRs, which lowers the series resistance of the mirror stacks. Since oxidation rate is strongly dependent on the Al content, the grading of the interfaces causes the oxidation rate to be reduced near the interfaces.

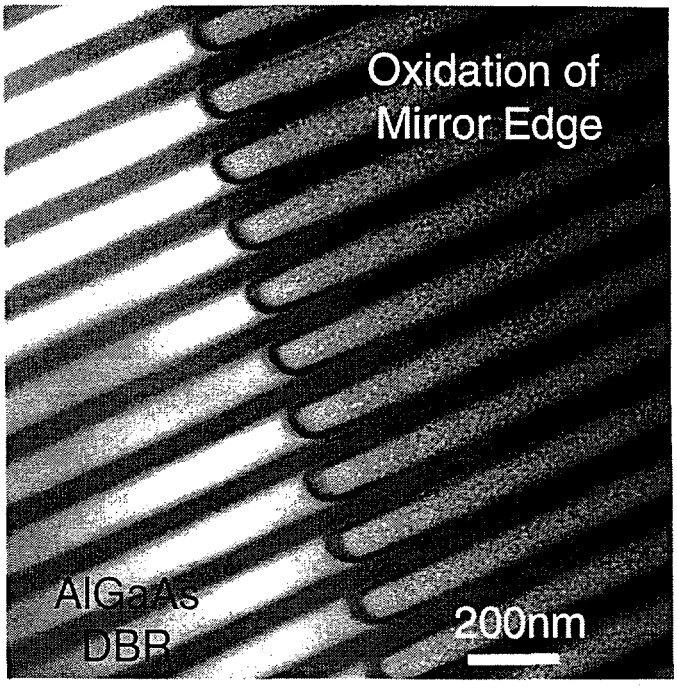

Figure 6: Bright-field strain contrast image of the oxidized portion of the DBR mirror stack. Some strain associated with the oxidation front is seen, but it does not propagate into the rest of the mirror. Also, no extended defects are seen emanating from the oxidation front.

The lattice image in Figure 5 shows a smooth transition from the unoxidized crystal to the oxidized amorphous zone. The exact position of the interface cannot be determined because the oxidation front is not exactly aligned with the crystal axes. However, it can be seen that the interface is smoothly varying without any sharp spikes into the crystal. In lower magnification strain contrast images (Figure 6), strain can be seen around the oxide fronts. However, the strain is confined to approximately one DBR period within the mirrors, and no extended defects have been seen emanating from the oxide front.

To form a fully dense γ-Al_2O_3 layer from AlAs would require a 20% linear contraction of the layer[12]. However, internal strains and a possible amorphous matrix would reduce this requirement. We have directly measured this contraction by comparing oxidized and unoxidized portions of a DBR mirror[8]. By measuring the change in position of the 18th mirror pair, the linear contraction is determined as 6.3% for the 8%-Ga Al_2O_3. The contraction occurs over an approximately 2μm-wide transition region behind the oxidation front. Thus, the region nearest the oxidation front is under a higher tensile strain than the rest of the DBR. While some relaxation is expected to occur during TEM sample preparation, the contraction of the oxidized layers is seen prior to sample preparation on the surface of the VCSEL devices using differential-interference contrast optical microscopy. The amount of contraction in the single, 2%-Ga Al_2O_3 layer was not measured due to the difficulty in assigning the exact position of the $Al_{0.98}Ga_{0.02}As$/GaAs interfaces, which were intentionally graded to lower the resistivity of the DBR mirrors. Also, the amount of contraction is expected to be less due to the rigidity of the surrounding, unoxidized material.

As stated earlier, the Al-Ga-O system is known to form solid solutions of Al_2O_3 /Ga_2O_3. Hence, it is expected that the Ga will remain in the in the oxidized layer $(Al_xGa_{1-x})_2O_3$. The

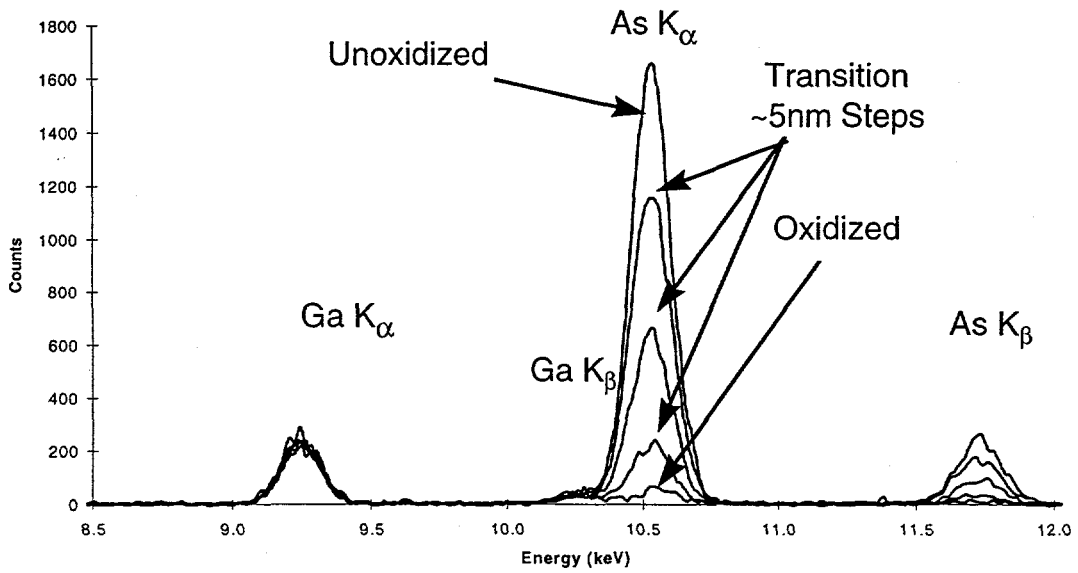

Figure 7: Portion of EDXS scan from the region around the oxide terminus. The Ga signal remains constant (as does the Al signal, not shown) while the As signal smoothly decreases to almost zero in the oxide.

disposition of the As is not as clear. It has been reported that AsH_3 is detected in the waste stream during bulk oxidation of AlAs[13], but during lateral oxidation, it is not clear that the As can escape. Using EDXS, we have measured the constituents in the region of the oxide terminus. The Al and Ga signal remained constant; however, the As signal was reduced to less than 2% in the oxidized portion of the layer as seen in Figure 7. In the transition from oxidized to unoxidized, we see a smooth decrease in the As signal, indicating the As is not enriched at the oxidation front. However, the probe size used (~10nm) is not small enough to resolve any fine structure at the reaction front.

We had recently reported that there were amorphous inclusions associated with the rapid oxidation of the 2%-Ga AlAs layers[8]. We have determined that these inclusions are, in fact, electron-beam-induced artifacts. They probably represent local, e-beam-induced crystallization of the amorphous matrix, causing a local contraction of the layer. This local contraction then leaves behind the low density pockets observed. This is consistent with the amorphous matrix being a lower density hydroxide phase.

CONCLUSIONS

While oxide confined VCSELs have recently demonstrated record device performances[3,4,5], the microstructure of the oxide layer defining the aperture has not been fully studied. We have performed TEM studies of the microstructure of the oxidized layers in VCSEL device structures and have begun to obtain a more complete understanding.

The crystalline phase observed in the oxidized layers is γ-Al_2O_3, which is stable against further oxidation. In addition to the crystalline γ-Al_2O_3, an amorphous matrix is present in the layers. This matrix is presumably a hydroxide or the amorphous rho-phase of alumina, and probably acts as a precursor to the γ-Al_2O_3 crystallites. This is supported by images of the oxide terminus, which show a purely amorphous zone between the oxidized and unoxidized

portion of the layers. This zone may act to passivate dangling bonds at the interface and help account for the high efficiencies of these devices.

The $Al_{0.92}Ga_{0.08}As$ layers contracted linearly by 6.3% after oxidation, but no extended defects were observed emanating from the oxidation front. This contraction of the oxide may have the biggest impact in high index-contrast DBR mirror applications utilizing GaAs/oxidized-AlAs layer pairs. Since the reflectivity band of these mirrors depends strongly on the layer thickness, a contraction of the oxidized layers would affect these mirrors. The oxide contraction does not seem to be a large problem in the present VCSEL application since the oxidized portion of the device is not dimensionally critical to its performance and the strain associated with the contraction does not generate defects in the device. This may not be the case when using pure AlAs rather than 2%Ga-AlAs as the current confining layer, since these devices are exceptionally vulnerable to mechanical failure[14].

ACKNOWLEDGMENTS

The authors wish to gratefully acknowledge the support of the United States Department of Energy under contract DE-AC02-94AL85000.

REFERENCES

[1] J. M. Dallessasse, N. Holonyak, Jr., A. R. Sugg, T.A. Richard and N. El-Zein, Appl. Phys. Lett. **57**, 2844 (1990).
[2] K. D. Choquette, K. L. Lear, R. P. Schneider, Jr., K. M. Geib, J. J. Figiel, and R. Hull, IEEE Photonics Technol. Lett. **7**, 1237 (1995)..
[3] D.L. Huffaker, D.G. Deppe, K. Kumar, and T.J. Rogers, Appl. Phys. Lett. **65**, 97 (1994).
[4] K. D. Choquette, R. P. Schneider, Jr., K. L. Lear, and K. M. Geib, Electron Lett. **30**, 2043 (1994).
[5] G.M. Yang, M.H. MacDougal, P.D. Dapkus, Electron Lett. **31**, 886 (1995).
[6] A. R. Sugg, E.I. Chen, N. Holonyak, K.C. Hsieh, J.E. Baker and N. Finnegan, J. Appl. Phys. **74** 3880 (1993).
[7] S. Guha, F. Agahi, B. Pezeshki, J.A. Kash, D.W. Kisker and N.A. Bojarczuk, Appl. Phys. Lett. **68**, 906 (1996).
[8] R.D. Twesten, D.M. Follstaedt, K. D. Choquette, and R. P. Schneider, Jr., Appl. Phys. Lett. **69**, 19 (1996).
[9] JCPDS file 10-425.
[10] B.C. Lippens and J.J. Steggerda in *Physical and Chemical Aspects of Adsorbents and Catalysts*, edited by B.G. Linsen (Academic Press, London, 1970) p.171-213.
[11] E.M. Levin, C.R. Robbins, and H.F. McMurdie, *Phase Diagrams for Ceramists,* (American Ceramic Society, Columbus, OH, 1970) Figure 310.
[12] The volume per Al atom in AlAs is $(3.57Å)^3$, while in γ-Al_2O_3 it is $(2.85Å)^3$ (for gibbsite, $Al(OH)_3$, it is $(3.49Å)^3$).
[13] H. Holonyak, private communication.
[14] K. D. Choquette, K. M. Geib, H.C. Chui. H.Q. Hou, and R. Hull, Mat. Res. Soc. Symp. Proc. **412** (1996) 53.